Dalton Transactions

Accepted Manuscript

ROYAL SOCIETY OF CHEMISTRY

www.rsc.org/dalton

Journal Name

RSCPublishing

ARTICLE

Enhanced $BaZrO_3$ mechanosynthesis by the use of metastable ZrO_2 precursors.

Cite this: DOI: 10.1039/x0xx00000x

Z. Sherafat[a,c], I. Antunes[b], C. Almeida[a], J. R. Frade[b], M. H. Paydar[c], G. C. Mather[d] and D. P. Fagg[a*]

Received 00th March 2014,
Accepted 00th March 2014

DOI: 10.1039/x0xx00000x

www.rsc.org/

The current work assesses the impact of structural differences between stable and metastable ZrO_2 precursors on the mechanochemical preparation of $BaZrO_3$. Monoclinic (m-ZrO_2) and tetragonal (t-ZrO_2) zirconia polymorphs were prepared without stabilizing additives by slow alkaline precipitation. High-energy milling of the individual ZrO_2 precursors induced different partial transformations in each case. The as-synthesized m-ZrO_2 powders showed partial conversion to the tetragonal polymorph on mechanical activation, reaching about 10% t-ZrO_2 after 420 min accompanied by increases in strain. In contrast, the as synthesized t-ZrO_2 powders underwent the inverse transformation to the monoclinic phase, producing about 50% m-ZrO_2 after 120 min with the liberation of strain. The t-ZrO_2 precursor was shown to exhibit the higher reactivity with barium peroxide, yielding significantly earlier formation of barium zirconate under room-temperature mechanosynthesis. The progress of the mechanochemical formation of $BaZrO_3$ has been discussed with respect to the differing behaviour of the ZrO_2 precursors upon mechanical activation and associated thermodynamic perspectives.

1- Introduction

Perovskite proton-conducting oxides have been widely investigated because of their promising applications in a variety of electrochemical devices such as fuel cells, steam electrolysis, hydrogen separation and hydrogen sensors [1-4]. Among them, barium zirconate has been suggested to offer important benefits for such applications because of its chemical stability and high bulk conductivity [5,6]. However, preparation of dense barium zirconate ceramics is far from trivial, especially from powders obtained by solid-state reaction due to the necessity of multiple regrinding and refiring steps to ensure homogeneity, resulting in poor sinterability of the final powders [7-10]. Thus, a range of soft chemical techniques have been proposed for the synthesis of barium zirconate-based powders, such as coprecipitation [11,12], oxidant-peroxo [13], combustion [14-16], spray pyrolysis [17,18] and the Pechini method [19]. All of these techniques require subsequent heat treatment to achieve pure phases, due to the formation of $BaCO_3$ during synthesis.

In contrast, mechanosynthesis can lead to the formation of reactive, nanosized, single phase powders at room temperature [22-30], which can be sintered to dense pellets at relatively low temperatures, and which can be prepared without the formation of significant quantities of $BaCO_3$ [23,24]. Although high-energy milling has been successfully employed for synthesizing $BaZr_{1-x}Y_xO_{3-\delta}$ materials, where $x > 0$, it is less effective for preparation of the stoichiometric composition ($x = 0$), due to the persistence of ZrO_2 impurities, even after extended milling times [25].

Monoclinic ZrO_2 is one of the main precursors used for synthesizing barium zirconate-based electrolyte by solid-state methods and was the precursor adopted for mechanosynthesis of the stoichiometric composition, $x = 0$, in the previous study of $BaZrO_3$ mechanosynthesis by the current authors [25]. The high-energy milling process mechanically activates the ground powder due to increases in both specific surface energy and elastic-strain energy. Various relaxation processes can dissipate this increase in free energy, such as heating, particle fracture, aggregation, surface adsorbtion, polymorphic modification and chemical reactions [31,32]. In this respect, one should note that ZrO_2 is susceptible to polymorphic transformation, adopting a monoclinic crystal structure at room temperature and transforming to tetragonal and cubic symmetries at respectively higher temperatures [33-38]. Moreover, zirconia is a very refractory oxide and the relaxation of activation free energy by the formation of chemical products has previously been characterised to progress through the formation of intermediate products that are deficient in the hardest precursor [39,40]. This factor may offer a possible explanation for the persistence of zirconia after long hours of mechanochemical treatment in the preparation of $BaZrO_3$ [25]. It is, therefore, clear that the progression of mechanochemical reactions will be highly dependent on the nature and behaviour of the selected precursors.

As the tetragonal polymorph of zirconia is thermodynamically stable at temperatures higher than 1170ºC and highly metastable at room temperature, stabilizing oxides are usually added to retain the tetragonal phase to low temperatures [41,42]. Nonetheless, several preparation routes have been documented that can produce the metastable tetragonal phase of pure, undoped ZrO_2 at room temperature. These processes typically consist of precipitation of hydrous zirconia with ammonia or triethanolamine from a zirconium salt solution that leads to amorphous zirconia that is crystallized by subsequent thermal treatment of the hydrous zirconia precipitate. By changing the concentration of zirconium salt solution, adding H_2O_2 to the solution and sulphation of precipitated zirconia before heat treatment, it is possible to form metastable tetragonal zirconia at room temperature without adding stabilizing dopants [43-45].

Hence, the main purpose of the present work is firstly to demonstrate true differences in the mechanical activation of stable and metastable zirconia polymorphs, without stabilizing additives, under high-energy milling. The second objective is to use tetragonal ZrO_2 as a precursor for synthesizing barium zirconate by high-energy milling for the first time and to compare and contrast the progression of mechanochemical reaction to that obtained using monoclinic ZrO_2. In order to investigate only the effect of the zirconia structure on the progress of reaction, monoclinic and tetragonal zirconia polymorphs have been prepared with similar particle size and the milling has been performed under the same conditions for both zirconia polymorphs.

2- Experimental

Zirconia samples were prepared by slow alkaline precipitation, using an inorganic salt, $ZrOCl_2.8H_2O$ (Sigma-Aldrich, 95% purity) as the starting reactant. A stock solution of salt with a concentration of 0.1 M was used to prepare monoclinic zirconia. After stirring, ammonia solution (Fluka) was added until the pH value of 10 was reached. The precipitate was filtered and washed with distilled water and subsequently dried at 90 ºC for 24 h. A calcination treatment was performed at 550 ºC for 5 h. For the preparation of tetragonal zirconia, H_2O_2 (Sigma-Aldrich, 30% wt. in H_2O) was added to the salt solution to give a molar ratio of ZrO_2 to H_2O_2 equal to 1:4. For the precipitation of gels, ammonia solution (Fluka) was added until the pH reached a value of 9. The gels were subsequently aged for 30 min, then filtered and washed with distilled water until no Cl^- ion was detected in the filtered water ($AgNO_3$ test). The powder was then dried at 110 ºC for 12 h. The dried powder was sulphated by adding 3 ml of 1 N H_2SO_4 (Sigma-Aldrich) per gram of powder and stirring at room temperature. The sulphated powder was dried at 110 ºC for 12 h and then calcined at 600 ºC for 4 h.

The particle size, morphology and crystal structure of the prepared powder were determined by surface area measurements, scanning electronic microscopy (SEM) and X-ray diffraction analysis (XRD), respectively.

High-energy milling experiments of ZrO_2 polymorphs, t-ZrO_2 and m-ZrO_2, were performed independently, in order to assess the structural and microstructural changes during mechanical activation of the precursors, and to provide information of their potential impact during the mechanosynthesis of barium zirconate.

High-energy milling was carried out in a planetary ball mill (Retsch PM200) in air at 650 rpm, using 125 cm^3 tetragonal zirconia vials with internal diameter 6cm (Retsch) and tetragonal zirconia balls of diameter 5 and 10mm, in equal number (Tosoh Co.). The ball-to-powder weight ratio was fixed at 10:1. Milling was performed in a series of 5 min steps with 5 min of interruption for cooling and the direction of rotation was reversed after each interruption. Samples were collected during milling, at regular periods of time, and characterized by XRD, using a Rigaku Geigerflex diffractometer (CuKα radiation, step width 0.02º, scan rate 0.5 º/min), over the angular range 10 - 80º (2θ). Weight fractions of t-ZrO_2 and m-ZrO_2 were calculated as a function of milling time by quantitative Rietveld analysis, using the FULLPROF program [46] in order to determine the extent of transformation of the zirconia polymorphs during milling. The crystallite size and lattice strain of ZrO_2 powders with different milling times, were estimated from the average size-strain plot, based on the integral-breadth method [47]. XRD line profiles were modelled by a Pearson VII distribution function (program Winfit 1.2.1 [48]) in order to determine the profile parameters. The instrumental contribution to line broadening was determined using LaB_6 as standard reference.

The synthesized m-ZrO_2 or t-ZrO_2 powders were combined with barium peroxide (Sigma-Aldrich, ≥ 95% purity), in stoichiometric quantities to prepare powders of $BaZrO_3$ (BZO). The precursors were milled in a planetary ball mill under the same operating conditions used in the high-energy milling experiments of zirconia, described above. The milling was performed for up to 420 min. The weight fractions of crystallized phases of the reaction mixture and the amorphous contribution were determined by quantitative Rietveld analysis of XRD patterns of samples collected during milling using a similar method to that documented previously [49]. Ni was used as internal standard for the correction of weights, and interpolation of background points was employed to model the amorphous contribution to the patterns. In addition, the fraction of unreacted precursors after mechanosynthesis of $BaZrO_3$, starting from the different ZrO_2 polymorphous, was estimated by thermogravimetric analysis (TGA) to 1200ºC using the Netzsch Jupiter instrument in dry argon atmosphere with a heating and cooling rate of 5 ºC/min..

3- Results and discussion

3.1- Synthesis of zirconia polymorphs

Figure 1 shows the XRD patterns of synthesized tetragonal and monoclinic zirconia powders. It can be seen that the formation of pure t-ZrO_2 phase is achieved at room temperature. SEM images of the ZrO_2 polymorphs powders show spherical agglomerates, consisting of particles with sizes in the nanometric range, Fig.2. The particle sizes determined by specific BET surface-area measurements were approximately 15 nm for t-ZrO_2 and 27 nm for m-ZrO_2. The close match in the particle size for each ZrO_2 precursor powder facilitates the subsequent comparison of these materials during mechanical milling.

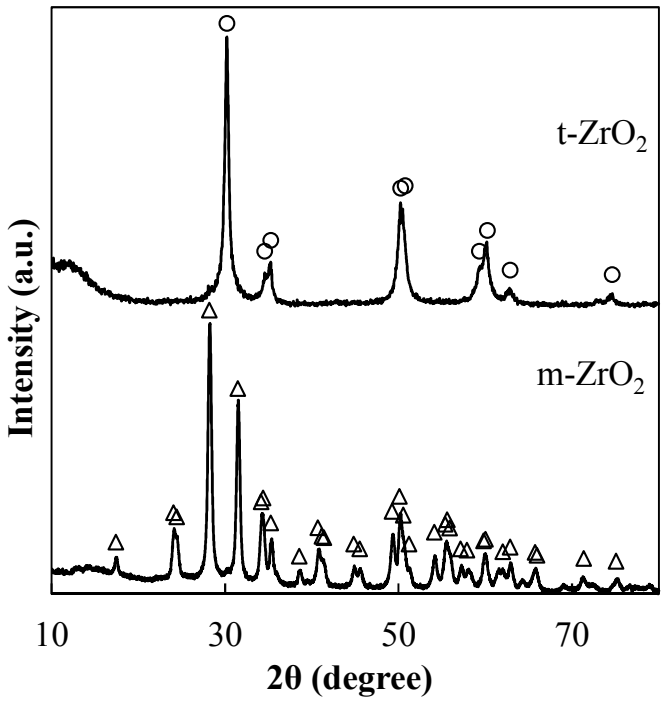

Figure 1. XRD patterns of the synthesized zirconia powders. The markers identify: (△) m-ZrO_2; (○) t-ZrO_2.

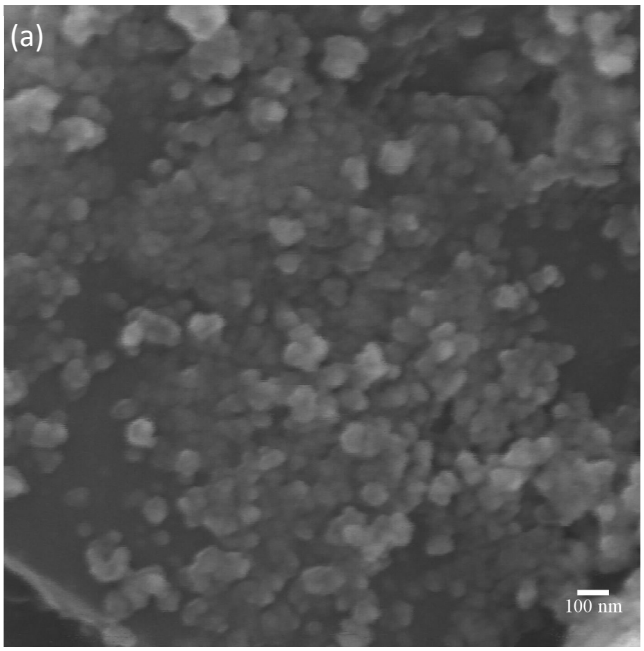

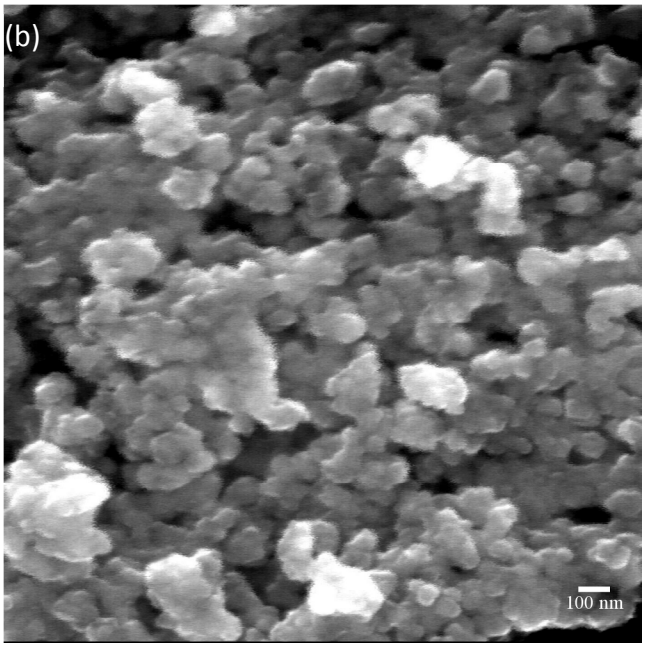

Figure 2. SEM images of (a) monoclinic zirconia and (b) tetragonal zirconia powders mounted on carbon tapes.

3.2-Transformation of zirconia polymorphs under high-energy milling

Figure 3 shows the XRD patterns of t-ZrO_2 after different milling times, while the time dependence for the conversion of t-ZrO_2 to m-ZrO_2 is indicated in Figure 4 as a function of decreasing t-ZrO_2 content.

It can be seen that transformation is fast during the initial hours of milling and conversion of t-ZrO_2 to m-ZrO_2 reaches almost 50 % (w/w) after 120 min, according to the Rietveld quantitative phase analysis (Figure.4). For longer milling times, the rate of transformation decreases and the fraction of residual tetragonal phase tends to a plateau.

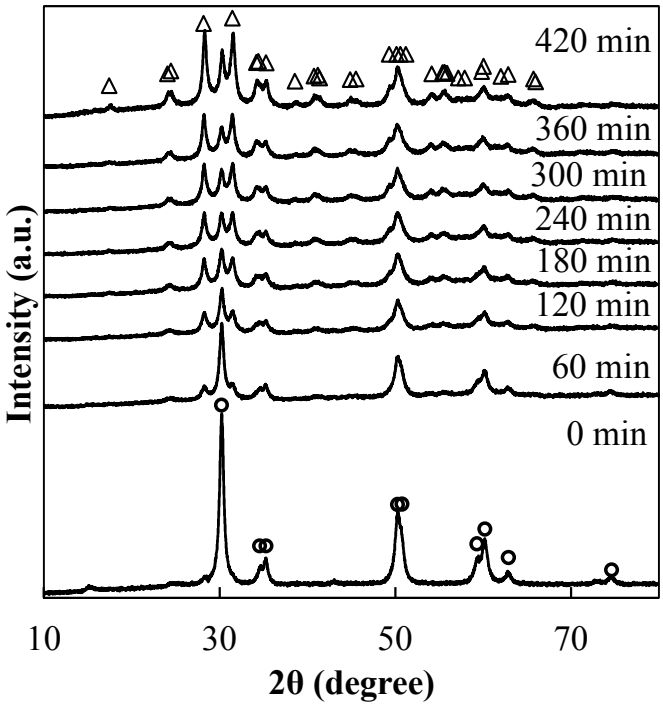

Figure 3. XRD patterns of t-ZrO_2 powders after different milling times. The markers identify: (△) m-ZrO_2; (○) t-ZrO_2.

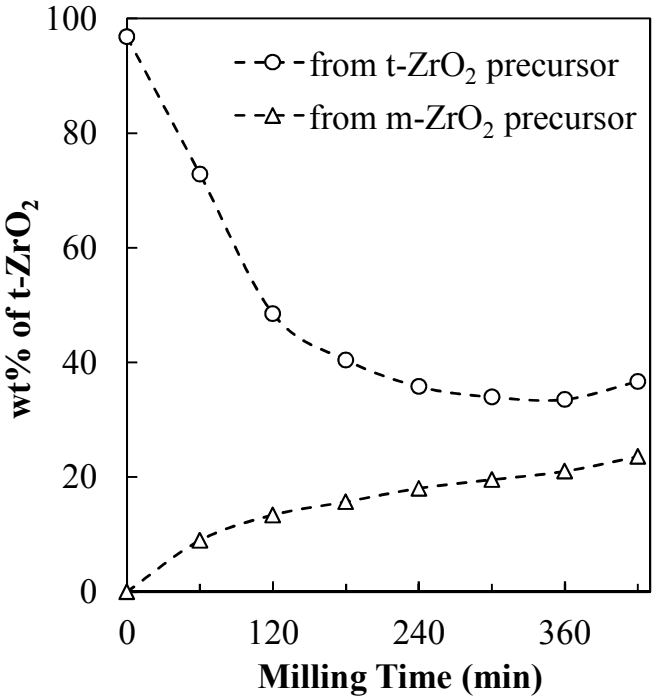

Figure 4. Weight fractions of t-ZrO2 as a function of milling time starting from monoclinic zirconia (△) and tetragonal zirconia (○) precursors.

XRD patterns of monoclinic zirconia precursor after different milling times are presented in Figure 5 and show the slow appearance of the tetragonal phase. Thus, while the t-ZrO_2 precursor is shown to rapidly decrease in quantity, converting partially to m-ZrO_2 on milling, the m-ZrO_2 precursor demonstrates the inverse behaviour, partially converting to the higher symmetry tetragonal phase on mechanical milling. The progression of the m-ZrO_2 to t-ZrO_2 transformation is presented in Figure 4. The rate of transformation of m-ZrO_2 to t-ZrO_2 is shown to be almost constant after 120 min. up to the longest milling time (420 min). Moreover, the polymorphic modification of the monoclinic zirconia precursor upon high-energy milling is shown to be slower than that of the inverse transformation of the tetragonal precursor. Conversion of m-ZrO_2 to t-ZrO_2 only reaches about 20% (w/w) after 420 min milling time in comparison to the modification of greater than 60% (w/w) t-ZrO_2 to m-ZrO_2 in the case of the tetragonal precursor, in the same time period (Figure 4). Determination of the amount of amorphous phase in the cases of the monoclinic and tetragonal precursors indicated that the amount of amorphous phase after a milling time of 420 min. was effectively negligible.

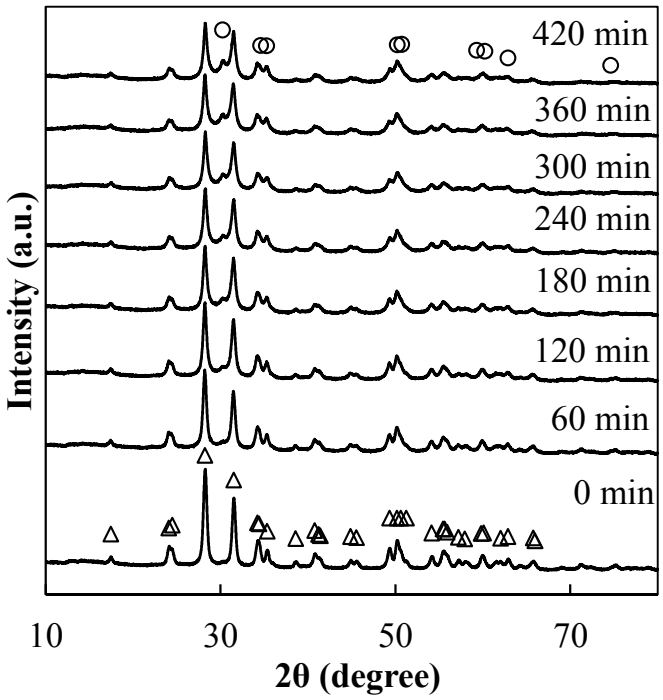

Figure 5. XRD patterns of m-ZrO_2 powders after different milling times. The markers identify: (△) m-ZrO_2; (○) t-ZrO_2.

The XRD patterns also reveal additional changes associated to peak broadening, which may arise due to the combined effects of changes of crystallite size in the nanometric range, lattice strain and significant residual microstrain. The contributions to integral-breadth of crystallite size and the strains can be evaluated by the adoption of an integral-breadth method relating the crystallite size, expressed as the average apparent diameter, ε, with the mean value of the strain, η [25,47]:

$$\left(\frac{\beta^*}{d^*}\right)^2 \approx \frac{1}{\varepsilon}\frac{\beta^*}{\left(d^*\right)^2}+\left(\frac{\eta}{2}\right)^2 \quad (1)$$

where $\beta^* = \beta\cos\theta/\lambda$ and $d^* = 2\sin\theta/\lambda$. β and d are the integral breadth and the interplanar distance, respectively. η is related with the root-mean-square strain (e_{rms}) by $e_{rms} = \eta/5$; this is shown in Figure 6 for the m-ZrO_2 precursor after different milling times. Results for 300 and 420 min of milling are not shown because the fitted data give excessively high errors for long milling times (above 40% for e_{mrs}). Similar difficulties have also been reported by other authors and are suggested to be due to very low particle sizes and amorphization [50,51]. In the current case, difficulties also arise because de-convolution of XRD peaks is affected by the close proximity of coexisting tetragonal and monoclinic polymorph reflections after extended milling.

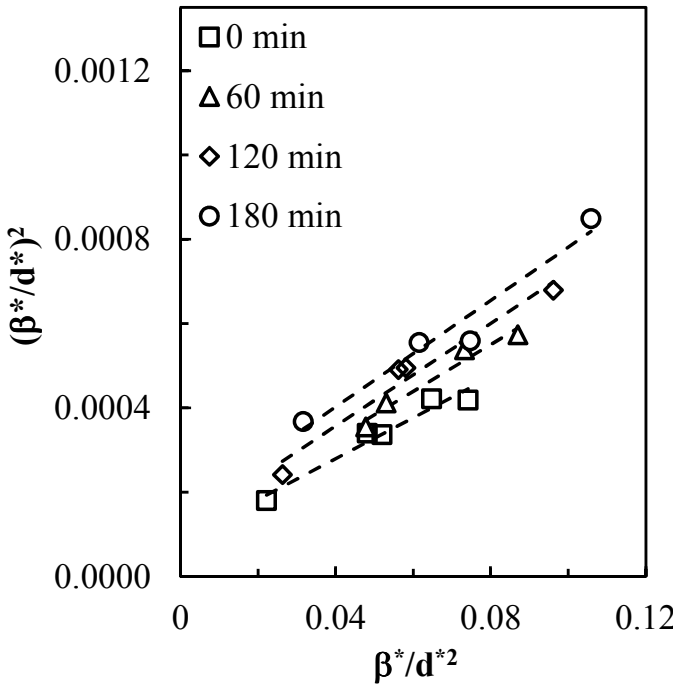

Figure 6. Size-strain plot of m-ZrO_2 before milling and after 60, 120 and 180 min of high-energy milling.

The crystallite size and the mean value of the strain can be estimated from the fitted linear data of the graphic representation of equation (1), based on the slope and y-intercept values, respectively. The results of average crystallite size and root-mean-square strain, e_{rms}, are shown in Figure 7, for m-ZrO_2. One firstly notes a close correlation between the calculated crystallite sizes and those previously recorded by the BET technique. The average crystallite size is shown to decrease slightly with increasing milling time. The percentage error associated with the determination of average crystallite size is in the range 11 - 23% as shown by the error bars in Figure 7. The corresponding values of strain exhibit notable increases with milling time, a trend that is typical of mechanochemical activation [31,32].

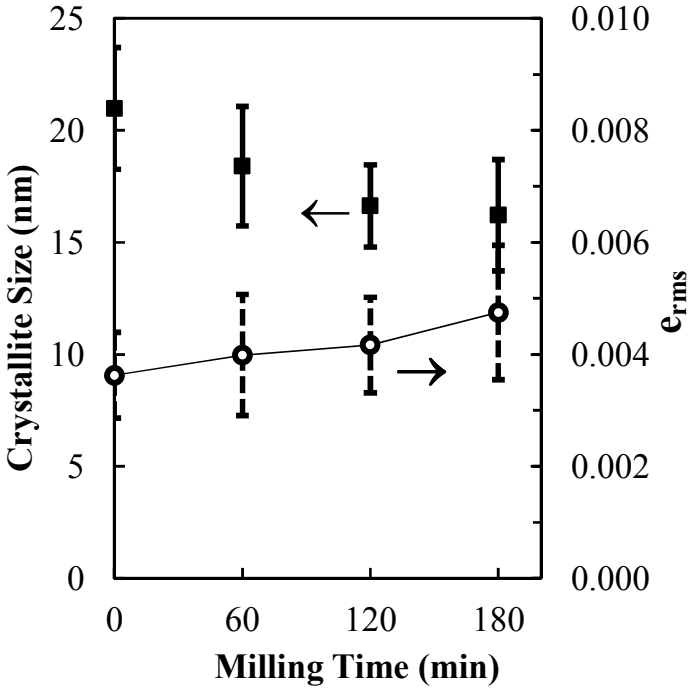

Figure 7. Average crystallite size (■) and root mean square strain, e_{rms}, (○) determined from the size-strain plot as function of milling time for m-ZrO_2.

The size-strain plots of t-ZrO_2 after different milling times (Figure 8) proved to be complex to analyse due to the rapid conversion of t-ZrO_2 to the monoclinic polymorph. Note that after 60 min and 120 min of milling the t-ZrO_2 precursor, the samples contain about 27% and 51% of m-ZrO_2, respectively (Figure 4). Thus, only the main reflections of the tetragonal phase were considered in order to minimize the risks of overlapping of XRD reflections of both m-ZrO_2 and t-ZrO_2.

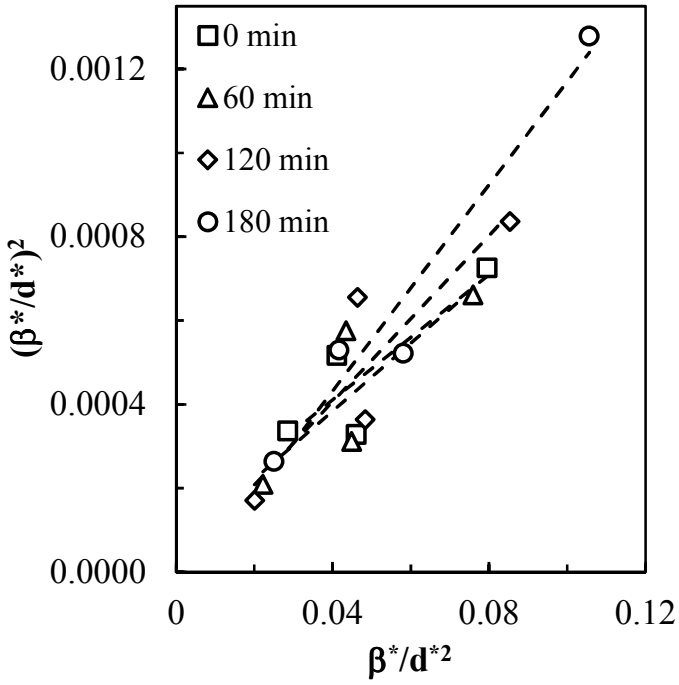

Figure 8. Size-strain plot of t-ZrO_2 before milling and after 60 and 120 and 180 min of high energy milling.

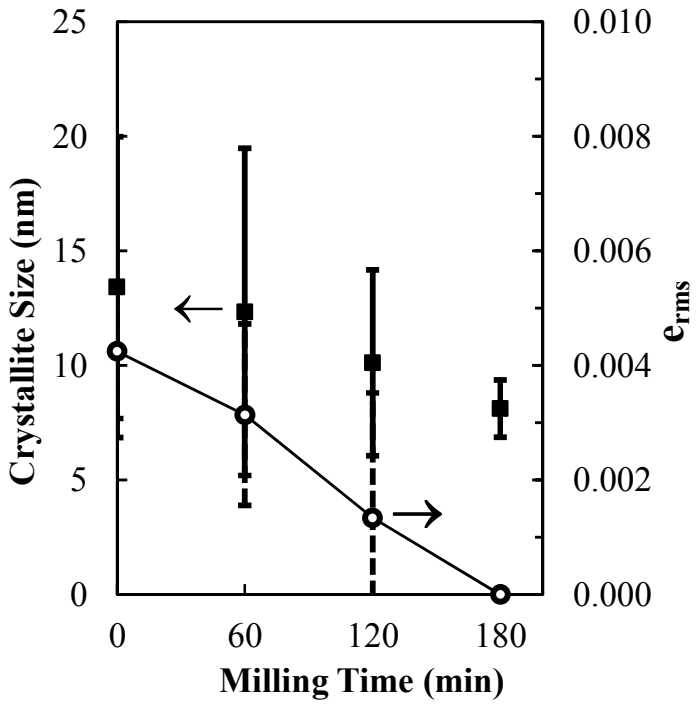

Figure 9. Average crystallite size (■) and root mean square strain, e_{rms}, (○) determined from the size-strain plot as function of milling time for t-ZrO_2.

Figure 9 shows the average crystallite size calculated from the slope of the size-strain plot for t-ZrO_2. The values of crystallite size for t-ZrO_2 before milling agree well with the particle sizes measured by BET. The results upon milling suggest significant grain refinement, and although major errors are associated with these estimates, it may be assumed that effects of high-energy milling of t-ZrO_2 powders include a prevailing contribution to partial transformation to m-ZrO_2 combined with decreases in crystallite size and strain. Note that the observation of decreasing strain with milling time in the t-ZrO_2 precursor is in contrast to the increasing strain noted in the case of m-ZrO_2. As stated in the introduction, various relaxation processes can dissipate the increase in specific surface and elastic-strain energies induced by mechanical activation. One of these is polymorphic transformation [31,32]. Upon polymorphic transformation of t-ZrO_2 to m-ZrO_2 though high-energy milling of the t-ZrO_2 precursor, the associated strain energy appears to decrease in agreement with this hypothesis.

3.3- Mechanosynthesis of $BaZrO_3$

The XRD patterns in Figure 10 show the evolution of barium zirconate as a function of milling time using t-ZrO_2 and BaO_2 as precursors, while the dependence of weight fraction of $BaZrO_3$ on the time of high-energy milling is summarised in Figure 11. It can be seen that the formation of $BaZrO_3$ from these precursors is very fast and traces of precursor reactants cannot be seen in the X-ray diffractograms after only 120 min. This can be ascribed to the high reactivity of metastable t-ZrO_2 powders on high-energy milling, as shown above. One should also note that no m-ZrO_2 can be observed during milling, Figure 10, suggesting that mechanical activation in the current case leads directly to chemical synthesis rather than phase modification. The presence of minor quantities of $BaCO_3$, observable after 60 min milling time, result from the high reactivity of BaO_2 and exposure of powder to atmospheric CO_2 either during milling or before XRD can be performed. This is discussed further in the section 3.4.

The evolution of mechanosynthesis of $BaZrO_3$ by using m-ZrO_2 and BaO_2 as the reaction-mixture precursors is presented in Figure 12 as a function of milling time. The fraction of formed $BaZrO_3$, evaluated by quantitative Rietveld analysis of XRD data, is also summarised in Figure 11. By using m-ZrO_2 as the precursor, the rate of BZO formation is distinctly slower than that using t-ZrO_2, as starting material. Note also that the XRD pattern still shows traces of the main reflection of m-ZrO_2 after the longest milling time (Figure 12). The small traces of barium carbonate peaks, which can be observed in the XRD patterns after 360 and 420 min of milling, can also be ascribed to reaction of BaO_2 with atmospheric CO_2, indicating that conversion of BaO_2 is incomplete even after the longest milling time when using the m-ZrO_2 precursor.

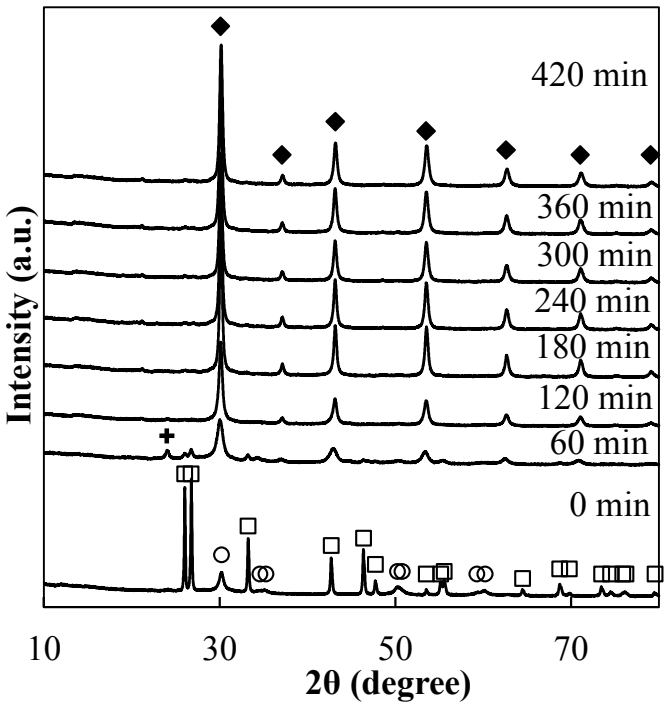

Figure 10. XRD patterns of $BaZrO_3$ after different milling time using t-ZrO_2 as a precursor. The markers identify: (□) BaO_2; (○) t-ZrO_2; (+) $BaCO_3$; (◆) $BaZrO_3$.

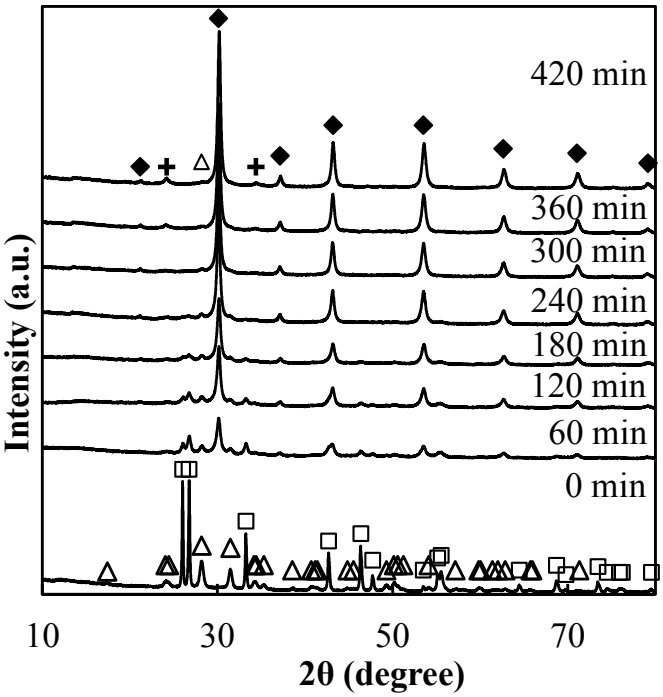

Figure 12: XRD patterns of $BaZrO_3$ after different milling time using m-ZrO_2 as a precursor. The markers identify: (□) BaO_2; (△) m-ZrO_2; (+) $BaCO_3$; (◆) $BaZrO_3$.

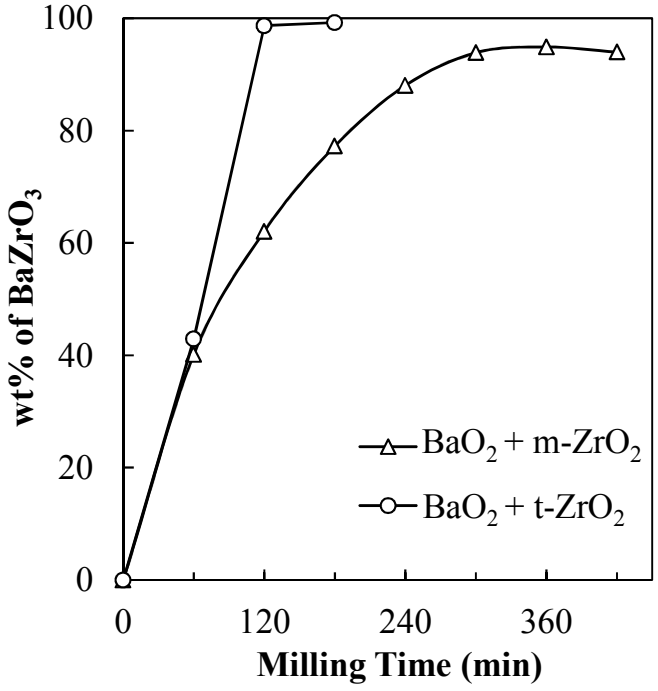

Figure 11. Weight fraction of $BaZrO_3$ as a function of milling time for mixtures of barium peroxide with different zirconia precursor polymorphs.

In order to assess the yield obtainable by room-temperature mechanosynthesis under these conditions, the amount of amorphous phase was determined by Rietveld refinement of the XRD patterns after 420 min of milling for each set of precursors, Table 1.

It can be seen that yields of $BaZrO_3$ of approximately 82% and 78% can be obtained from the precursors, t-ZrO_2-BaO_2 and m-ZrO_2-BaO_2, respectively, under these milling conditions. Further assessment of yield was performed by thermogravimetry (Figure 13). The initial stage of weight loss starts at room temperature, reaches a maximum rate at temperatures below 100 ºC and slows down to a minimum rate at T ≈ 315 ºC for t-ZrO_2-BaO_2/$BaZrO_3$ mixtures and at T≈375ºC for m-ZrO_2-BaO_2/$BaZrO_3$. This stage may be ascribed to losses of adsorbed humidity. A second stage shows increasing rate of weight losses until a maximum at about T ≈ 630 ºC for t-ZrO_2-BaO_2/$BaZrO_3$ and T ≈ 660ºC for m-ZrO_2-BaO_2/$BaZrO_3$; most likely related to decomposition of residual barium peroxide, which is expected to occur in this temperature range [52]. One may even assume further formation of barium zirconate during the heating schedule of thermogravimetry, mainly because the fraction of weight uptake on subsequent cooling is much smaller than on heating; this suggests that the fraction of unreacted precursors nearly vanishes after the peak temperature. This observation coincides with that of our earlier paper on $BaZrO_3$ mechanosynthesis where complete reaction could be obtained by calcination of mechanosynthesised powders [25]. The measured weight losses of the second stage were, therefore, used to estimate the fraction of residual (amorphous) barium peroxide after mechanosynthesis of barium zirconate. It was thus concluded that the yield of barium zirconate was about 86% for the t-ZrO-BaO_2/$BaZrO_3$ mixtures, and slightly lower, 80%, for m-ZrO_2-BaO_2/$BaZrO_3$. The incomplete conversion of the precursors to the final $BaZrO_3$ product explains the

observation of traces of barium carbonate in Figure 12 even after long milling times. In addition, the slower formation of the $BaZrO_3$ phase in the m-ZrO_2-BaO_2 case may increase the time available for carbonate formation, a factor that possibly contributes to the differences in final yield.

Table 1. Weight percentages of $BaZrO_3$, $BaCO_3$ and amorphous phase after room-temperature mechanosynthesis for each set of precursors.

	t-ZrO_2-BaO_2 (%w/w)	m-ZrO_2-BaO_2 (%w/w)
$BaZrO_3$	81.5	77.7
$BaCO_3$	-	8.3
Amorphous	18.5	14

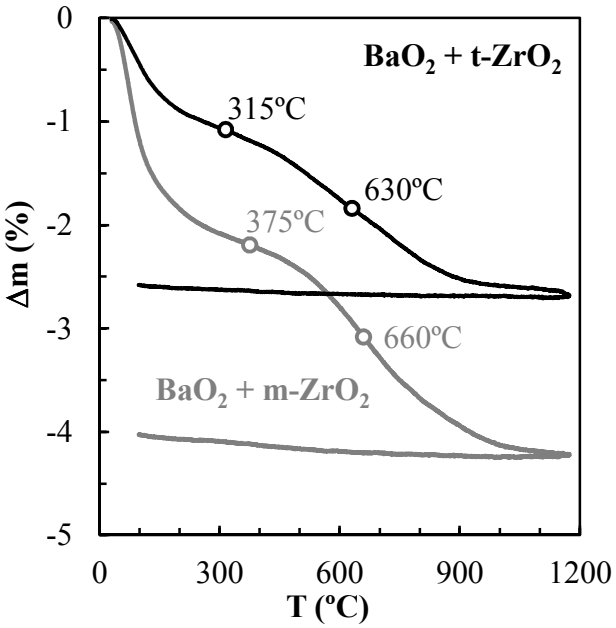

Figure 13. TGA plot of $BaZrO_3$ powders obtained by mechanosynthesis from BaO_2–t-ZrO_2 and BaO_2–m-ZrO_2 powder mixtures, heated and cooled under a dry Ar atmosphere, at a rate of 5 ºC/min.

3.4- Thermodynamic analysis

Chemical-potential diagrams were plotted as described elsewhere [53-55]. These diagrams were used as thermodynamic guidelines for the relevant ternary system ZrO_2-BaO-O_2 (Figure 14) to assess conditions required for reactivity.

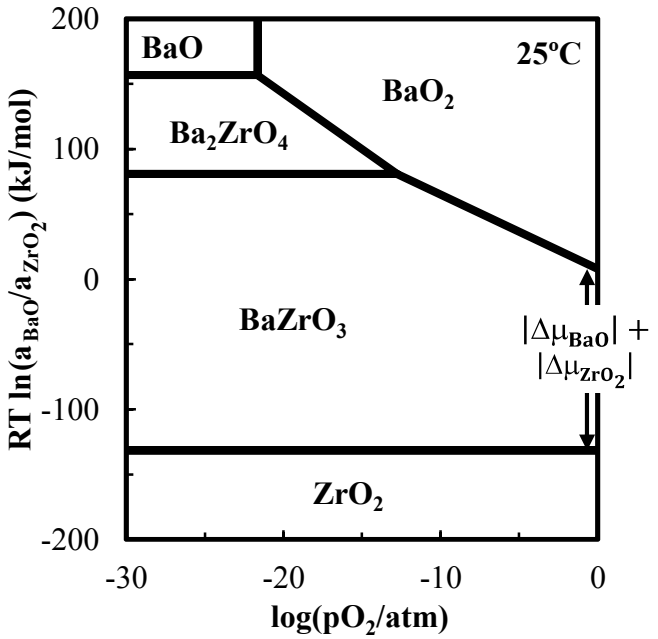

Figure 14. Chemical-potential diagram for the system ZrO_2-BaO-O_2 at 25ºC.

Figure 14 confirms that reactivity of zirconia with barium peroxide is promoted by very favourable thermodynamic conditions, even at room temperature. Note that the chemical potential ratio shown in Figure 14 combines the gradients of chemical potentials of both oxide components:

$$R\,T\,\Delta\log\left(\frac{a_{BaO}}{a_{ZrO_2}}\right) = R\,T\,\Delta\log\left(a_{BaO}\right) - R\,T\,\Delta\log\left(a_{ZrO_2}\right)$$

$$= \Delta\mu_{BaO} - \Delta\mu_{ZrO_2}$$

Thus, the difference marked in Figure 14 can be considered as a driving force for solid-state kinetics, including diffusion controlled kinetics when reactants are separated by a layer of reaction product [56]. Note also that arrows in Figure 14 mark the chemical potential differences across a model series association ZrO_2/$BaZrO_3$/BaO.

The chemical-potential difference marked in Figure 14 is at least one order of magnitude higher than the typical range of transition enthalpy for transformation of tetragonal and monoclinic zirconia, which is reported to be in the order of 5-10 kJ/mol [41]. Thus, the transition enthalpy between the t-ZrO_2 and m-ZrO_2 polymorphs is too small to play a major role in the observed solid-state kinetics. The greater reactivity of tetragonal zirconia should, therefore, be ascribed mainly to its greater ability to undergo the dissipation of mechanical activation, possibly related to the release of strain energy upon phase transformation and subsequent promotion of chemical synthesis. This is consistent with the well-known disruptive nature of this phase transformation, due to loss in symmetry and the high anisotropy of elastic properties [57]. On the contrary, for the m-ZrO_2-BaO_2 mixture, one may assume that mechanical activation contributes mainly to an increase in strain energy, as shown above.

Figure 15 shows the corresponding chemical-activity diagrams for the ternary system ZrO_2-BaO-CO_2, which explain why barium zirconate cannot be obtained from ZrO_2-$BaCO_3$ powder mixtures, except possibly under high vacuum. The predictions for 500 ºC show a typical lower limit for onset of barium zirconate in CO_2-rich atmosphere, as expected when reaction of $BaCO_3$ and ZrO_2 occurs in nearly closed atmosphere. Thus, high-energy milling of ZrO_2-$BaCO_3$ mixtures is very unlikely to yield barium zirconate, even if one considers that mechanical attrition may cause significant heating.

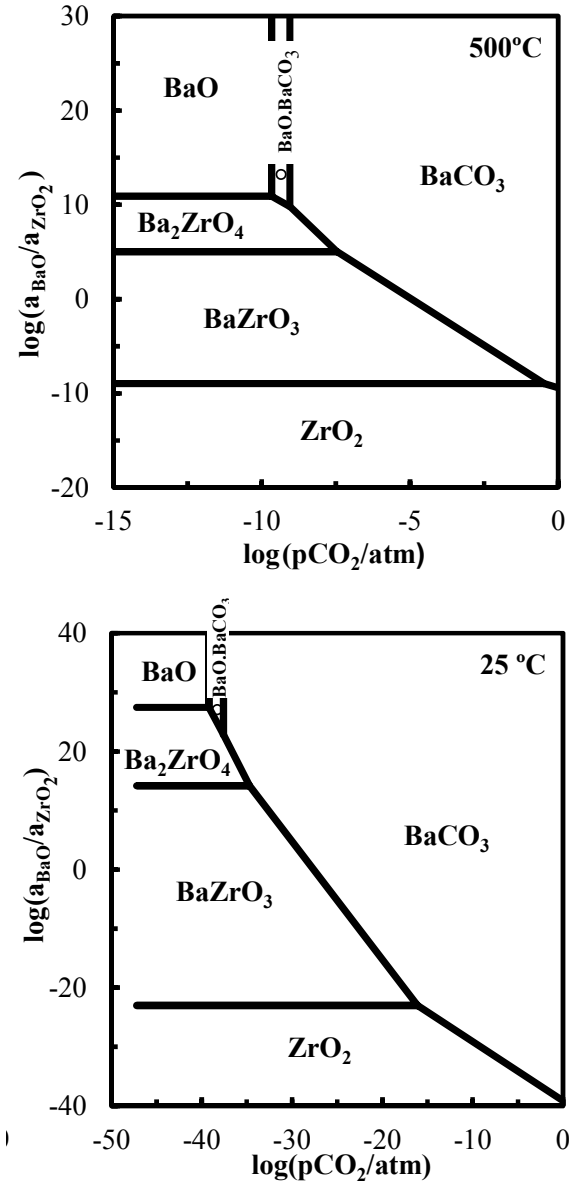

Figure 15. Chemical-activity diagrams for the ZrO_2-BaO-CO_2 system at 500ºC and at room temperature.

The observation of barium carbonate during mechanical activation of t-ZrO_2-BaO_2 (Figure 10) and m-ZrO_2-BaO_2 mixtures (Figure 12) is also supported by thermodynamics (Figure 16). Though barium peroxide is redox stable down to quite reducing conditions, it is very prone to react with atmospheric CO_2 that has a typical partial pressure in the order of 400 ppm. The basic barium carbonate $BaO.BaCO_3$ is expected only in a narrow range of conditions, and is unlikely to occur even as intermediate reaction product. Carbonate should, thus, be the main reaction product and conversion of barium peroxide to barium carbonate is, probably, only limited by slow kinetics at both room temperature and on heating to intermediate temperatures. In this respect, one should note that the decomposition of BaO_2 upon high-energy milling will liberate oxygen. This factor may lower the pCO_2 experienced in the closed vials and may explain why XRD only shows traces of barium carbonate and much more intense XRD peaks of barium zirconate. On the other hand, one should not neglect the role of high energy mechanical activation on these solid-gas reactions. There is clear evidence that mechanical activation induces significant structural changes on peroxides and carbonates, facilitating subsequent thermal decomposition [58-60]. Finally, the slower conversion to the $BaZrO_3$ phase in the m-ZrO_2-BaO_2 case can also be expected to lead to an increased risk of carbonate formation.

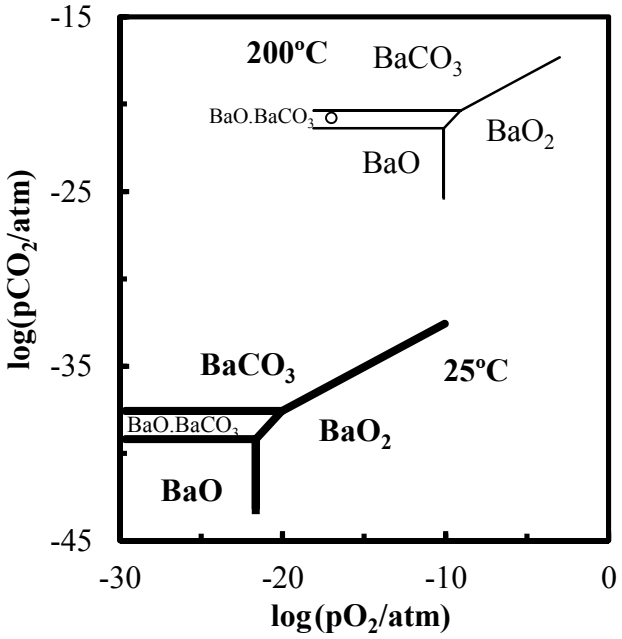

Figure 16. Chemical-activity diagrams for the BaO-CO_2-O_2 system at 25ºC (thick lines) and 200ºC (thin lines).

Conclusions

The tetragonal and monoclinic polymorphs of zirconia show quite different behaviours upon high-energy mechanical activation. Faster transformation of the metastable tetragonal precursor is observed, yielding substantial quantities of the monoclinic phase after short milling times. In contrast, mechanical activation of the m-ZrO_2 precursor shows a slow transformation to small quantities of the tetragonal polymorph, even after relatively long milling times. The integral-breadth method applied to the XRD patterns, after different milling

times, suggests a slight decrease in crystallite size for both t-ZrO_2 and m-ZrO_2 precursors upon milling. In the case of m-ZrO_2, milling also leads to increases in strain. In contrast, the rapid polymorphic change to lower symmetry on milling the t-ZrO_2 precursor appears to liberate the strain associated with mechanical activation. This metastable tetragonal precursor also yields faster conversion to barium zirconate by mechanochemical reaction with barium peroxide, with extinction of XRD peaks of the reactants after about 120 min. Reaction of monoclinic zirconia with barium peroxide is shown to be considerably slower and XRD patterns of the reacting mixture still reveal traces of zirconia after long milling times. Rietveld refinement of the fraction of amorphous phases after 420 min milling time and TG analysis both indicate $BaZrO_3$ yields of around 80%, with a slightly higher yield noted for the t-ZrO_2 precursor. The fractions of unreacted amorphous peroxide are highly prone to reaction with atmospheric CO_2, forming the stable barium carbonate. The progress of mechanically activated changes is shown to be consistent with thermodynamic predictions.

Acknowledgements

The authors acknowledge financial support from the FCT/COMPETE/FEDER (Portugal) under projects PTDC/CTM/100412/2008, PTDC/CTM/105424/2008. Isabel Antunes is thankful to the FCT for doctoral research grant SFRH/BD/76738 /2011. Glenn Mather acknowledges the support of grants funded by MINECO (ENE2012-30929) and CSIC (i-link0743).

Notes and references

[a] Nanotechnology Research Division, Centre of Mechanical Technology and Automation, Department of Mechanical Engineering, University of Aveiro, 3810-193 Aveiro, Portugal.

[b] Department of Materials and Ceramic Engineering, CICECO, University of Aveiro, 3810-193 Aveiro, Portugal.

[c] Department of Materials Science and Engineering, School of Engineering, Shiraz University, Shiraz, Iran

[d] Institute of Ceramics and Glass, CSIC, Cantoblanco, 28049 Madrid, Spain.

1 H. Iwahara, T. Esaka, H. Uchida and N. Maeda, *Solid State Ionics*, 1981, **3**, 359.

2 H. Iwahara, H. Uchida and N. Maeda, *J. Power Sources*, 1982, **7**, 293.

3 H. Iwahara, *Solid State Ionics*, 1988, **28**, 573.

4 T. Kobayashi, K. Abe, Y. Ukyo and H. Matsumoto, *Solid State Ionics*, 2001, **138**, 243.

5 K.D. Kreuer, S. Adams, W. Munch, A. Fuchs, U. Klock and J. Maier, *Solid State Ionics*, 2001, **145**, 295.

6 Y. Yamazaki, R. Hernandez-Sanchez and S. M. Haile, *Chem. Mater.*, 2009. 21, 2755.

7 R.C.T. Slade, S.D. Flint and N. Singh, *Solid State Ionics*, 1995, **82**, 135.

8 H. Matsumoto, S. Okada, S. Hashimoto, K. Sasaki, R. Yamamoto, M. Enoki and T. Ishihara, *Ionics*, 2007, **13**, 93.

9 S. Tao and J.T.S. Irvine, *J. Sol. State Chem.*, 2007, **180**, 3493.

10 J.-S. Park, J.-H Lee, H.-W. Lee and B.-K. Kim, *Solid State Ionics*, 2010, **181**, 163.

11 J. Brzezinska-Miecznik, K. Haberko and M.M. Bucko, *Mater. Lett.*, 2002, **56**, 273.

12 F. Boschini, B. Robertz, A. Rulmont and R. Cloots, *J. Eur. Ceram. Soc.*, 2003, **23**, 3035.

13 M.D. Gonçalves and R. Muccillo, *Ceram. Int.*, 2014, **40**, 911.

14 P. Babilo and S.M. Haile, *J. Am. Ceram. Soc.*, 2005, **88**, 2362.

15 P. Babilo, T. Uda and S.M. Hailea, *J. Mater. Res.*, 2007, **22**, 1322.

16 E. Fabbri, L. Bi, H. Tanaka, D. Pergolesi and E. Traversa, *Adv. Funct. Mater.*, 2011, **21**, 158.

17 M.M. Bucko and J. Oblakowski, *J. Eur. Ceram. Soc.*, 2007, **27**, 3625.

18 P.A. Stuart, T. Unno, R. Ayres-Rocha, E. Djurado and S.J. Skinner, *J. Eur. Ceram. Soc.*, 2009, **29**, 697.

19 H.J. Park, *J. Solid State Electrochem.*, 2011, **15**, 2205.

20 A. Magrez and T. Schober, *Solid State Ionics*, 2004, **175**, 585.

21 G. Taglieri, M. Tersigni, P.L. Villa and C. Mondelli, *Int. J. Inorg. Mater.*, 1999, **1**, 103.

22 V.V. Zyryanov, V.A. Sadykov, N.F. Uvarov, G.M. Alikina, A.I. Lukashevich, S. Neophytides and J.M. Criado, *Solid State Ionics*, 2005, **176**, 2813.

23 P. Gonçalves and F.M. Figueiredo, *Solid State Ionics*, 2008, **179**, 991.

24 A. Moure, A. Castro, J. Tartaj and C. Moure, *Ceram. Int.*, 2009, **35**, 2659.

25 Antunes, A. Brandao, F.M. Figueiredo, J.R. Frade, J. Gracio and D.P. Fagg, *J. Sol. State Chem.*, 2009, **182**, 2149.

26 M.J. Sayagués, J.M. Córdoba and F.J. Gotor, *J. Sol. State Chem.*, 2012, **188**, 11.

27 V. Šepelák, A. Düvel, M. Wilkening, K.-D., Becker, P. Heitjans, *Chem. Soc. Rev.*, 2013, **42**, 7507.

28 V. Šepelák, S. Bégin-Colin, G. Le Caër, *Dalton Trans.*, 2012, **41**, 11927.

29 T. Friščić, I. Halasz, P.J. Beldon, A.M. Belenguer, F. Adams, S.A.J. Kimber, V. Honkimäki, R.E. Dinnebier, *Nat. Chem.*, 2013, **5**, 66.

30 P. Baláž, M. Achimovičová, M. Baláž, P. Billik, Z. Cherkezova-Zheleva, J.M. Criado, F. Delogu, E. Dutková, E. Gaffet, F.J. Gotor, R. Kumar, I. Mitov, T. Rojac, M. Senna, A. Streletskii, K. Wieczorek-Ciurowa, *Chem. Soc. Rev.*, 2013, **42**, 7571.

31 V.V. Boldyrev, S.V. Pavlov and E.L. Goldberg, *Int. J. Miner. Process.*, 1996, **44**, 181.

32 J. Lin, *J. Therm. Anal. Calorim.*, 1998, **52**, 453.

33 G. Štefanić, S. Musić, A. Gajović, *Mat. Res. Bull.,* 2006, **41**,764.

34 G. Štefanić, S. Musić, A. Gajović, *J. Eur. Ceram. Soc.*, 2007, **27**, 1001.

35 G. Štefanić, S. Musić, Croat. *Chem. Acta*, 2002, **75**,727.

36 J.E. Bailey, D. Lewis, Z.M. Librant, L.J. Porter, *Trans. J. Brit. Ceram. Soc.*, 1972, **71**, 25.

37 A.V. Chadwick, M.J. Pooley, K.E. Rammutla, S.L.P. Savin, A. Rogier, *J. Phys.:Condens. Mater*, 2003, 15, 431.

38 A.N. Scian, E.F. Aglietti, M.C. Caracoche, P.C. Rivas, A.F. Pasquevich, A.R. López García, *J. Am. Ceram. Soc.*, 1994**,** **77**, 1525.

39 V.V. Zyryanov, *Inorganic Materials*, 2005, **41**, 378.

40 V.V. Zyryanov, *Science of Sintering*, 2005, **37**, 77.

41 M. Chen, B. Hallstedt, L.J. Gauckler, *Solid State Ionics*, 2004, **170**, 255.

42 J.R. Kelly and I. Denry, *Dent. Mater.*, 2008, **24**, 289.

43 W. Stichert and F. Schuth, *Chem. Mater.*, 1998, **10**, 2020.
44 J.A. Navio, G. Colón, P.J. Sánchez-Soto and M. Macias, *Chem. Mater.*, 1997, **9**, 1256.
45 L.A. Pérez-Maqueda and E.Matijević, *J. Mater. Res*. 1997, **12**, 3286.
46 J. Rodriguez-Carvajal, *Abstracts of the Satellite Meeting on Powder Diffraction of the XV Congress of the IUCr.*; Toulouse, France., 1990.
47 J.I. Langford, D. Louër and P. Scardi, *J. Appl. Crystallogr.*, 2000, **33**, 964.
48 S. Krumm, *Mater. Sci. Forum*, 1996, **228**, 183.
49 A. De Pablos-Martín, G.C. Mather, F. Muñoz, S. Bhattacharyya, T. Höche, J.R. Jinschek, T, Heil, A. Durán and M.J. Pascual, *J. Non-Cryst. Solids*, 2010, **356**, 3071.
50 E. Rodríguez-Reyna, A.F. Fuentes, M. Maczka, J. Hanuza, K. Boulahya and U. Amador, *J. Sol. State Chem.*, 2006, **179**, 522.
51 A.F. Fuentes, K. Boulahya, M. Maczka, J. Hanuza and U. Amador, *Solid State Sciences*, 2005, **7**, 343.
52 M.J. Tribelhorn and M.E. Brown, *Thermochim. Acta*, 1995, **255**, 143.
53 H.Yokokawa, T. Kawada and M. Dokiya, *J. Amer. Ceram. Soc.*, 1989, **72**, 2104.
54 A. Brandão, J.F. Monteiro, A.V. Kovalevsky, D.P. Fagg, V.V. Kharton and J.R. Frade, *Solid State Ionics*, 2011, **192**, 16.
55 J.F. Monteiro, A.A.L. Ferreira, I. Antunes, D.P. Fagg and J.R. Frade, *J. Sol. State Chem.*, 2012, **185**, 143.
56 H. Smalzried, *Solid State Reactions*; Verlag Chemie, Weinheim, 1981.
57 M. Mamivand, M.A. Zaeem, H.E. Kadiri and L.-Q. Chen, *Acta Mater.*, 2013, **61**, 5223.
58 I.A. Massalimov, *Inorg. Mater.*, 2007, **43**, 1371.
59 I.A. Massalimov, A.U. Shayakhmetov and A.G. Mustafin, *Russ. J. Appl. Chem.*, 2010, **83**, 1794.
60 J.M. Criado, M.J. Dianez and J. Morales, *J. Materials Science*, 2004, **39**, 5189.

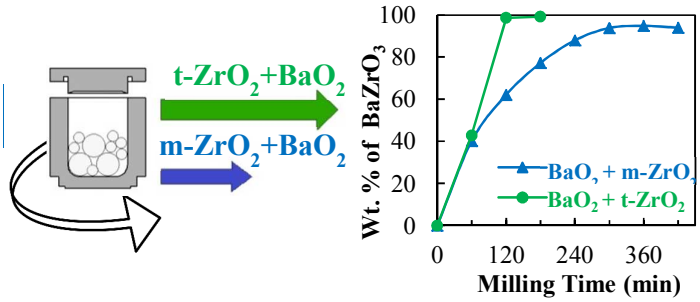

Enhanced mechanochemical preparation of $BaZrO_3$ can be achieved upon milling mixtures of barium peroxide with metastable tetragonal ZrO_2 precursors.